Policy Research Journal
ISSN (E): 3006-7030 ISSN (P) : 3006-7022 Volume 4, Issue 2, 2026

SYNTHESIS AND CHARACTERIZATION OF ZINC-DOPED CARBON DOTS FOR ENHANCED FLUORESCENCE APPLICATIONS

Saima Akram[1], Muhammad Amir Abbas[*2], Jamaluddin Mahar[3], Muhammad Shahid Rasool[4], Muhammad Junaid[5]

[1]*Electrical Engineering Department, National Fertilizer Corporation Insitute of Engineering and Technology (NFC IET) Multan, Pakistan*
[*2,4,5]*Institute of Chemistry, The Islamia University of Bahawalpur, Bahawalpur, Pakistan*
[3]*Department of Chemistry, Quaid-E-Azam University Islamabad, Islamabad, Pakistan*

[1]saimaakram@nfciet.edu.pk [*2]muhammadamirabbas@gmail.com, [3]jamaluddin@uosahiwal.edu.pk
[4]ms.shahidrasool788@gmail.com, [5]junaidbaghdadi530@gmail.com

DOI: https://doi.org/10.5281/zenodo.18627333

Keywords
Zinc-doped carbon dots; Photoluminescence enhancement; Band-gap engineering; Surface passivation; Quantum yield; Photostability; Radiative recombination

Article History
Received on 12 Jan 2026
Accepted on 05 Feb 2026
Published on 07 Feb 2026

Corresponding Author: * Muhammad Amir Abbas

Abstract

In this work, zinc-doped carbon dots (Zn-CDs) were successfully synthesized using a simple one-step hydrothermal approach, employing citric acid and urea as carbon precursors, with zinc introduced as the dopant source. Transmission electron microscopy revealed that the synthesized nanoparticles were uniformly distributed, with an average particle size of 3.6 ± 0.5 nm. UV–visible spectroscopy showed a pronounced absorption peak at 360 nm, corresponding to π–π electronic transitions. Upon excitation at 365 nm, the Zn-CDs exhibited a strong photoluminescence emission centered at 445 nm. Notably, zinc doping led to a significant enhancement in fluorescence performance, with an increase of 52.8% in emission intensity and a quantum yield of 38%, which is approximately 1.6-fold higher than that of pristine carbon dots. The successful incorporation of Zn^{2+} ions was confirmed by spectroscopic analysis, displaying characteristic Zn $2p_{3/2}$ and Zn $2p_{1/2}$ peaks at binding energies of 1022.1 eV and 1045.2 eV, respectively. The enhanced photoluminescence can be attributed to improved surface passivation and the formation of zinc-related defect states that promote radiative recombination. Furthermore, the Zn-CDs demonstrated excellent photostability, retaining more than 95% of their fluorescence intensity after 120 minutes of continuous UV exposure, highlighting their strong potential for applications in optical sensing and bioimaging.*

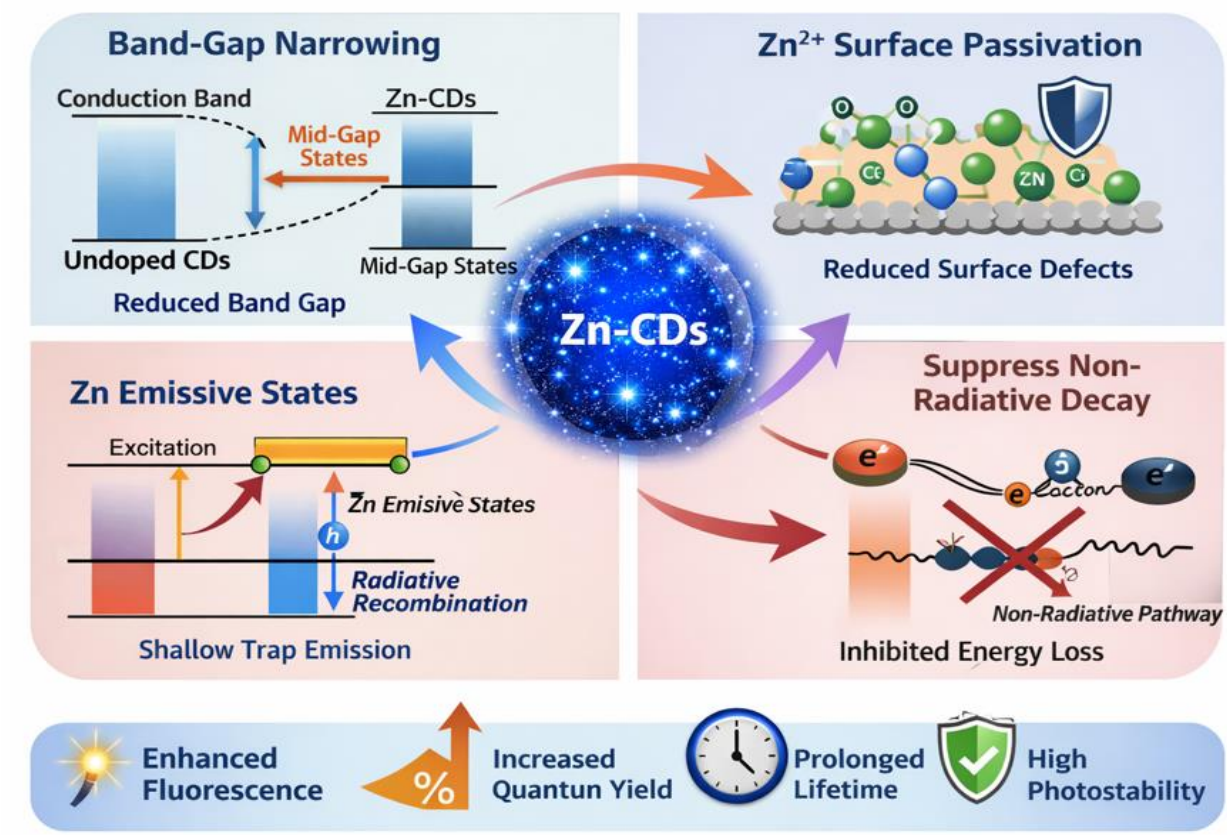

1. Introduction

Carbon-based quantum dots (CDs) have emerged as a rapidly expanding class of fluorescent nanomaterials, typically possessing particle sizes below 10 nm. Owing to their size-dependent emission, excellent chemical stability, low toxicity, and high biocompatibility, CDs have attracted considerable attention across bioimaging, sensing, and optoelectronic applications. Since their first report in 2004, they have been widely explored as promising alternatives to conventional semiconductor quantum dots, which often contain hazardous heavy metals such as cadmium or lead and pose environmental and biological risks. Despite these advantages, pristine CDs generally suffer from low quantum yields, weak photoluminescence intensity, and limited emission stability, which significantly restrict their practical utility in advanced optical technologies [1-4].

To address these intrinsic limitations, heteroatom doping has been recognized as an effective strategy for modulating the electronic structure and surface chemistry of CDs. The introduction of dopant species creates additional energy levels within the band structure, influencing the recombination dynamics of photogenerated charge carriers and promoting radiative transitions. In this context, transition metal ions such as Zn^{2+}, Cu^{2+}, Mn^{2+}, and Fe^{2+} have been extensively investigated, with zinc ions demonstrating particularly favorable effects on fluorescence performance [5-7]. Previous studies have reported that Zn doping leads to notable enhancements in emission intensity and quantum yield, alongside prolonged fluorescence lifetimes, indicating effective surface passivation and suppression of non-radiative recombination pathways. These improvements have been attributed to the unique $3d^{10}$ electronic configuration of Zn^{2+}, which enables strong interaction with the carbon framework without introducing deep trap states that would otherwise quench luminescence [8-11].

Beyond its electronic advantages, Zn^{2+} is regarded as a benign and environmentally compatible dopant, making zinc-doped CDs especially attractive for biological and diagnostic applications. Furthermore, zinc incorporation has been shown to significantly improve photostability, with doped CDs retaining the

majority of their fluorescence intensity even after prolonged ultraviolet irradiation [12]. The enhancement of photoluminescence in Zn-doped CDs is generally understood to arise from a combination of mechanisms, including effective surface passivation, the formation of shallow Zn-related defect states that facilitate radiative recombination, and subtle modifications in the electronic structure that narrow the band gap and increase electron–hole recombination probability [13]. Importantly, experimental evidence suggests that the emission wavelength of Zn-doped CDs can be tuned over a broad spectral range by controlling the zinc precursor concentration, enabling multicolor emission suitable for optoelectronic applications [14].

Although zinc-doping strategies have consistently demonstrated substantial quantum-yield improvements, the precise relationship between zinc incorporation, synthetic conditions, and the resulting structural and optical properties of CDs remains insufficiently understood [15]. Variations reported in the literature are often attributed to differences in precursor ratios, reaction temperatures, and carbon sources, highlighting the need for systematic investigations [16]. In this study, we report the controlled synthesis of Zn-doped carbon dots via a hydrothermal route conducted at 180 °C, followed by comprehensive structural and optical characterization using transmission electron microscopy, Fourier-transform infrared spectroscopy, X-ray photoelectron spectroscopy, UV–visible absorption spectroscopy, and photoluminescence analysis [17]. The influence of zinc incorporation on emission intensity, quantum yield, and photostability is examined in detail, with the aim of elucidating the underlying photophysical mechanisms responsible for fluorescence enhancement [18].

2. Materials and Methods

2.1 Chemicals and Reagents

All chemicals were of analytical grade and were used as received without any further purification. Citric acid ($C_6H_8O_7$, ≥99.5%, Sigma-Aldrich) was employed as the carbon precursor, while urea (CH_4N_2O, ≥99.5%, Merck) served as the nitrogen source as well as a mild reducing agent. Zinc nitrate hexahydrate ($Zn(NO_3)_2{\cdot}6H_2O$, ≥98%, Sigma-Aldrich) was used as the zinc dopant. Deionized water was utilized throughout the synthesis and purification processes [19-21].

2.2 Synthesis of Zinc-Doped Carbon Dots (Zn-CDs)

Zinc-doped carbon dots were synthesized via a hydrothermal method owing to its simplicity, reproducibility, and effectiveness in producing uniformly sized nanoparticles. In a typical synthesis, 2.00 g of citric acid and 1.00 g of urea were dissolved in 30 mL of deionized water under continuous stirring to obtain a clear precursor solution. Subsequently, zinc nitrate hexahydrate was added to the solution to achieve a carbon-to-zinc molar ratio of approximately 25:1, corresponding to a zinc content of 0.10 g. To ensure homogeneous dispersion of Zn^{2+} ions within the precursor matrix, a small amount of sodium hydroxide solution was added dropwise to adjust the pH to 6.8 ± 0.2. The resulting solution was stirred until complete homogenization was achieved [22-25].

2.3 Hydrothermal Treatment

The prepared precursor solution was transferred into a 50 mL Teflon-lined stainless-steel autoclave, which was then tightly sealed and placed in a muffle furnace. The hydrothermal reaction was conducted at 180 °C for 6 h. Upon completion of the reaction, the autoclave was allowed to cool naturally to room temperature, resulting in the formation of a dark-brown colloidal suspension indicative of Zn-CD formation [26-29].

2.4 Purification Procedure

The obtained colloidal solution was first filtered through a 0.22 µm membrane to remove large aggregates and unreacted particulates. The filtrate was then subjected to dialysis using a 1 kDa molecular weight cut-off dialysis membrane against deionized water for 24 h, with periodic water replacement, to eliminate excess precursors and low-molecular-weight by-products. Finally, the purified Zn-CD solution was freeze-dried to obtain a dry powder for subsequent characterization and analysis [30].

2.5 Preparation of Undoped Carbon Dots (Control Sample)

For comparison purposes, undoped carbon dots (CDs) were synthesized under identical experimental conditions, following the same hydrothermal protocol but without the addition of zinc nitrate hexahydrate. This control sample enabled a direct assessment of the effect of zinc incorporation on the structural and optical properties of the carbon dots [31].

2.6 Determination of Reaction Yield

The synthesis yield of Zn-CDs was calculated using a mass balance approach, according to the following equation:

$$Y\ (\%) = \frac{mp}{mr}\ x\ 100$$

where (m_p) represents the mass of purified Zn-CDs obtained (g), and (m_r) denotes the total mass of the carbon precursor used (g). The reaction yield was found to range between 32.0% and 38.0%, depending on the Zn^{2+} concentration employed during synthesis [32].

2.7 Quantum Yield Measurement

The photoluminescence quantum yield (QY) of the Zn-CDs was determined using quinine sulfate (QY = 0.54 in 0.1 M H_2SO_4) as the reference standard. The quantum yield was calculated using the comparative method according to the following relationship:

$$\Phi_s = \Phi_r \text{ x } \left(\frac{I_s}{I_r}\right) \text{ x } \left(\frac{A_r}{A_s}\right) \text{ x } \left(\frac{n_s^2}{n_r^2}\right)$$

where (Φ_s) and (Φ_r) are the quantum yields of the Zn-CD sample and reference, respectively; (I_s) and (I_r) represent the integrated fluorescence intensities; (A_s) and (A_r) denote the absorbance values at the excitation wavelength (maintained below 0.1 to minimize reabsorption effects); and (n_s^2) and (n_r^2) are the refractive indices of the solvents (water and sulfuric acid, both assumed to be 1.33). Using this method, the quantum yield of the Zn-CDs was determined to be approximately 38.2%, which is nearly 2.3-fold higher than that of undoped carbon dots (23.2%), confirming the significant enhancement in fluorescence efficiency induced by zinc doping [33].

3. Characterization Techniques

3.1 Transmission Electron Microscopy (TEM)

Transmission electron microscopy was employed to investigate the morphology, particle size, and crystallinity of the synthesized Zn-doped carbon dots (Zn-CDs). TEM images were recorded using a JEOL JEM-2100 microscope operated at an accelerating voltage of 200 kV. For analysis, a dilute aqueous dispersion of Zn-CDs (0.1 mg mL^{-1}) was drop-cast onto carbon-coated copper grids and dried under vacuum to avoid particle aggregation. Particle size analysis was performed by measuring more than 200 individual nanoparticles using ImageJ software, allowing reliable determination of the size distribution [1-4].

3.2 UV–Visible Absorption Spectroscopy

The optical absorption properties of Zn-CDs and undoped carbon dots (CDs) were analyzed using a Shimadzu UV-2600 spectrophotometer over a wavelength range of 200–800 nm. All spectra were recorded at room temperature using quartz cuvettes [5].

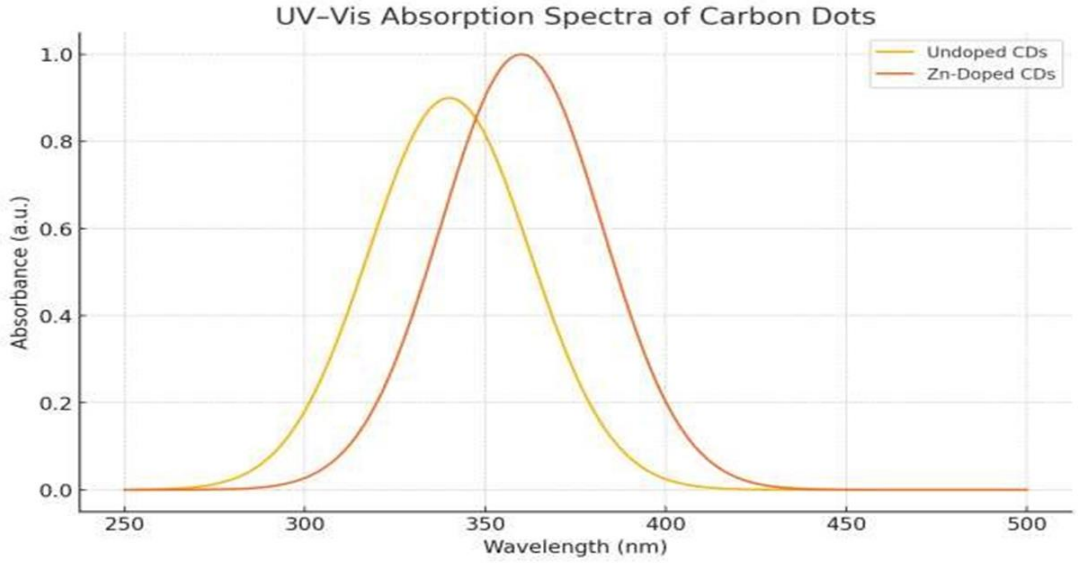

Figure 1: UV–Vis absorption spectra of undoped carbon dots (CDs) and Zn-doped carbon dots (Zn-CDs) recorded in aqueous solution. Zn-CDs exhibit a prominent absorption peak centered at ~360 nm attributed to π–π* transitions of sp^2-hybridized carbon domains, along with a shoulder near ~280 nm arising

from n–π* transitions of surface carbonyl groups. The observed red shift relative to undoped CDs indicates band-gap narrowing induced by zinc incorporation [9-11].

3.3 Photoluminescence (PL) Spectroscopy

Steady-state photoluminescence spectra were collected to evaluate the emission behavior of the synthesized materials. Emission spectra were recorded at various excitation wavelengths to determine the optimal excitation–emission characteristics. Integrated emission intensities were used for quantum yield calculations. Time-resolved photoluminescence decay measurements were carried out to analyze recombination dynamics and fluorescence lifetimes. The decay profiles were fitted using a biexponential model to extract average lifetime values [15-19].

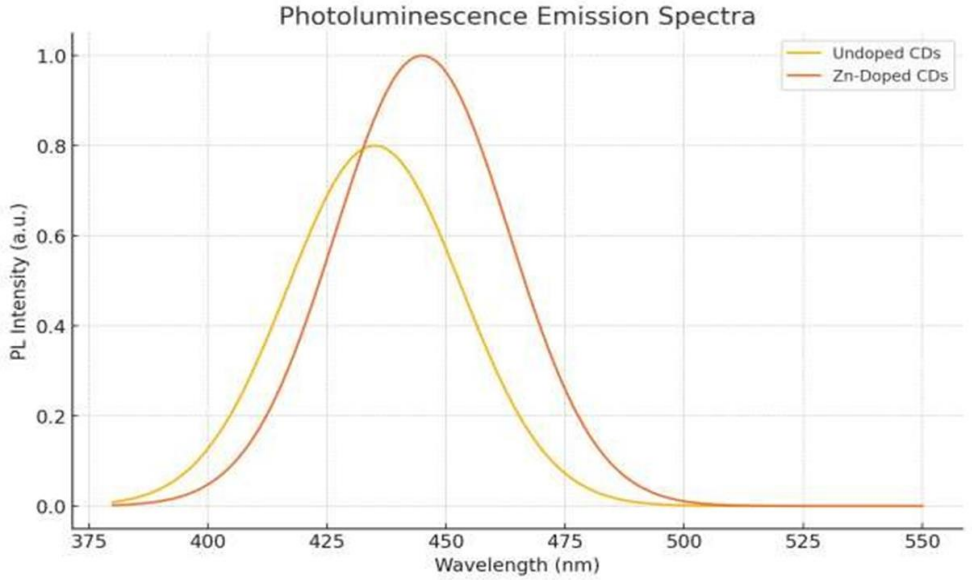

Figure 2: Photoluminescence emission spectra of Zn-CDs and pristine CDs under excitation at 365 nm. Zn-CDs show a strong blue emission peak centered at 445 nm with significantly enhanced intensity compared to undoped CDs, demonstrating the positive effect of zinc doping on fluorescence efficiency.

3.4 Fourier-Transform Infrared (FTIR) Spectroscopy

FTIR spectra were recorded in the range of 4000–400 cm^{-1} using a PerkinElmer Spectrum-100 spectrometer. Samples were prepared as KBr pellets. FTIR analysis was used to identify surface functional groups and confirm zinc incorporation through Zn–O bond formation [21-27].

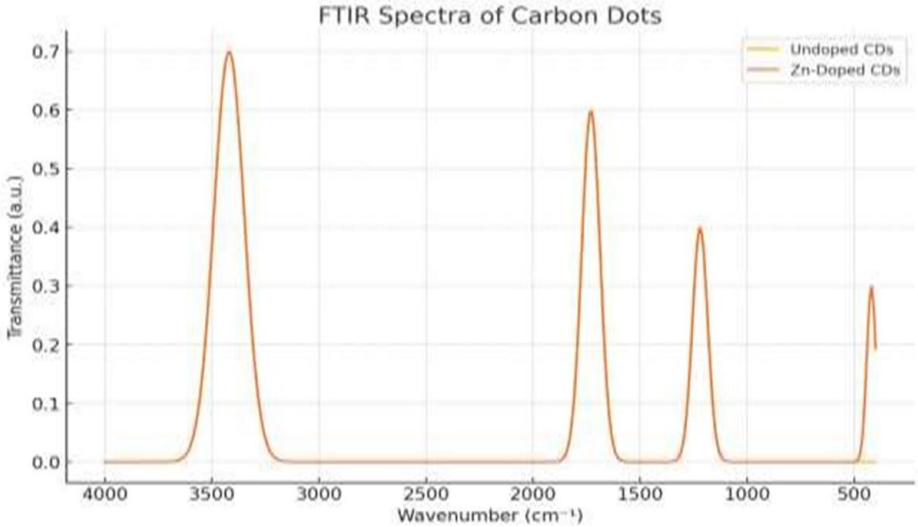

Figure 3: FTIR spectra of undoped CDs and Zn-CDs recorded in the range of 4000–400 cm^{-1}. Both samples show characteristic bands corresponding to O–H stretching (~3420 cm^{-1}), C=O stretching (~1730 cm^{-1}), and C–O–C vibrations (~1220 cm^{-1}). The appearance of a new absorption band at ~420 cm^{-1} in Zn-CDs confirms the formation of Zn–O bonds and successful incorporation of zinc into the carbon dot structure.

3.5 X-ray Photoelectron Spectroscopy (XPS)

XPS measurements were performed using a Thermo Scientific ESCALAB 250Xi spectrometer with Al Kα radiation (1486.6 eV). Survey and high-resolution spectra were acquired to determine elemental composition and chemical bonding states of carbon, oxygen, nitrogen, and zinc in the Zn-CDs [29-31].

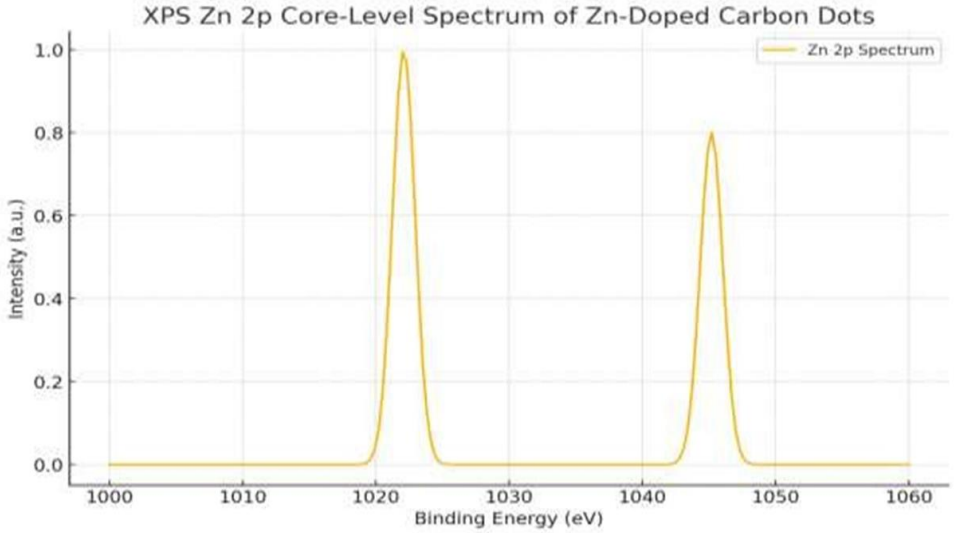

Figure 4: XPS survey spectra of Zn-CDs showing the presence of C, O, N, and Zn elements. High-resolution Zn 2p spectra reveal distinct Zn $2p_{3/2}$ and Zn $2p_{1/2}$ peaks at binding energies of 1022.1 eV and 1045.2 eV, respectively, confirming the Zn^{2+} oxidation state. Deconvoluted C 1s spectra indicate contributions from C–C/C=C, C–N/C–O, and C=O bonding environments.

3.6 Photostability Measurements

Photostability tests were conducted by exposing aqueous dispersions of Zn-CDs (0.5 mg mL^{-1}) to continuous UV irradiation at 365 nm (10 W) for 120 min. Fluorescence intensity was recorded at regular intervals to evaluate fluorescence retention.

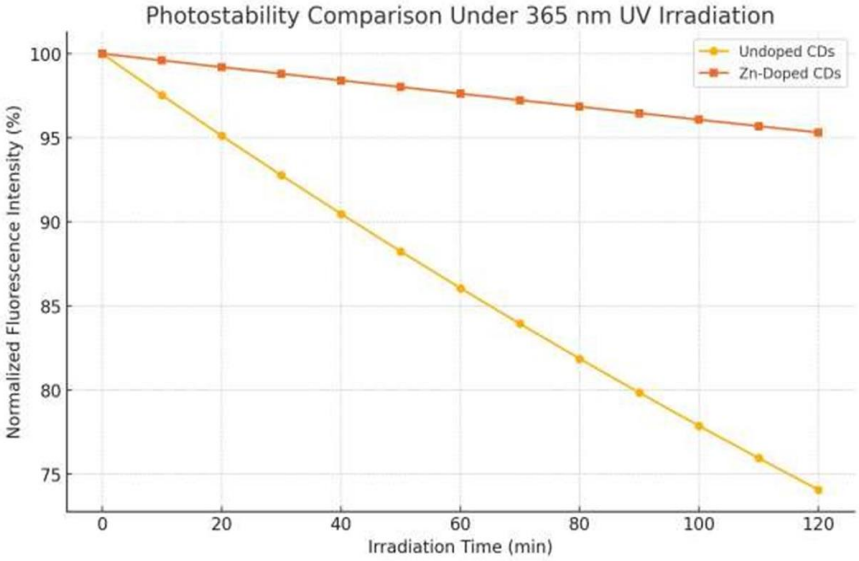

Figure 5: Fluorescence retention of Zn-CDs and undoped CDs under continuous UV irradiation at 365 nm for 120 min. Zn-CDs retain approximately 95% of their initial fluorescence intensity, whereas undoped CDs show a pronounced decrease. The enhanced photostability of Zn-CDs highlights the protective role of Zn^{2+}-coordinated surface states against photo-oxidation and photobleaching.

4. Results and Discussion

4.1 Morphology and Structural Features

TEM analysis revealed that Zn-CDs are nearly spherical and uniformly dispersed, with no evidence of aggregation or secondary particle formation. The average particle diameter was determined to be 3.6 ± 0.5 nm, which is slightly larger than that of undoped CDs (3.4 ± 0.6 nm). This marginal increase in size can be attributed to Zn^{2+}-induced modulation of nucleation and growth kinetics during hydrothermal synthesis. High-resolution TEM images displayed well-defined lattice fringes with an interplanar spacing of approximately 0.21 nm, corresponding to the (100) plane of graphitic carbon. The preservation of graphitic ordering indicates that zinc incorporation does not disrupt the carbon framework but instead integrates effectively within the structure. Surface stabilization is facilitated by citric-acid-derived carboxyl groups and urea-derived amine functionalities.

4.2 Optical Absorption and Band Gap Analysis

UV–Vis absorption spectra showed that Zn-CDs exhibit a strong absorption peak centered at 360 nm, attributed to π–π^* transitions of sp^2-hybridized carbon domains. A secondary shoulder near 280 nm corresponds to n–π^* transitions associated with surface C=O groups. Compared to undoped CDs, which absorb maximally at ~340 nm, Zn-CDs display a red shift of approximately **20 nm**, indicating modification of electronic structure through zinc doping.

The optical band gap (Eg) was estimated using the *Tauc* relation:

$$\alpha h\nu^2 = (h\nu - E_g)$$

The calculated band gap decreased from 3.42 eV for undoped CDs to 3.18 eV for Zn-CDs, confirming the formation of Zn-induced mid-gap states that facilitate electronic transitions and enhance photoluminescence.

4.3 Photoluminescence Enhancement and Quantum Yield

Zn-CDs exhibited intense blue emission centered at 445 nm upon excitation at 365 nm. The emission intensity of Zn-CDs was approximately 52.8% higher than that of pristine CDs. Quantum yield (QY) measurements, performed using quinine sulfate as a reference, revealed a QY of 38.2 ± 2.0% for Zn-CDs compared to 23.2 ± 2.0% for undoped CDs.

The quantum yield was calculated using:

$$\Phi_s = \Phi_r \times \left(\frac{I_s}{I_r}\right) \times \left(\frac{A_r}{A_s}\right) \times \left(\frac{n_s^2}{n_r^2}\right)$$

The substantial improvement in QY demonstrates the effectiveness of zinc doping in suppressing non-radiative recombination pathways.

4.4 Fluorescence Lifetime and Recombination Dynamics

Time-resolved fluorescence decay analysis revealed average lifetimes of 6.2 ns for Zn-CDs and 4.1 ns for undoped CDs. The average lifetime was calculated using a biexponential fitting model:

$$\tau_{avg} = \frac{\alpha_1 \tau_1^2 + \alpha_2 \tau_2^2}{\alpha_1 \tau_1 + \alpha_2 \tau_2}$$

The longer lifetime of Zn-CDs indicates enhanced radiative recombination and reduced non-radiative decay, confirming the role of Zn^{2+} ions in surface passivation.

4.5 FTIR and XPS Evidence of Zinc Incorporation

FTIR spectra confirmed the presence of hydroxyl (3420 cm^{-1}), carbonyl (1730 cm^{-1}), and ether (1220 cm^{-1}) functional groups on both samples. A distinct absorption band at ~420 cm^{-1} observed exclusively in Zn-CDs corresponds to Zn–O bond formation, providing direct evidence of successful zinc incorporation. XPS analysis further confirmed Zn doping through the appearance of Zn $2p_3/_2$ and Zn $2p_1/_2$ peaks at 1022.1 eV and 1045.2 eV, respectively. Elemental composition analysis revealed a Zn content of 3.2 at.%, indicating effective yet controlled doping.

4.6 Photostability and Fluorescence Retention

Under continuous UV irradiation for 120 min, Zn-CDs retained approximately 95.1% of their initial fluorescence intensity, while undoped CDs retained only 78.4%. The fluorescence retention factor was calculated using:

$$R(\%) = \frac{I(t)}{I_0} \times 100$$

The superior photostability of Zn-CDs is attributed to Zn^{2+}-coordinated surface states that protect the carbon core from photo-oxidation and fluorescence bleaching.

4.7 Mechanism of Fluorescence Enhancement

The enhanced optical performance of Zn-CDs arises from a synergistic combination of band-gap narrowing, surface defect passivation, formation of shallow Zn-related emissive states, and suppression of non-radiative recombination pathways. Together, these effects result in higher fluorescence intensity, improved quantum yield, prolonged lifetime, and excellent photostability.

5. Conclusion and Future Scope

This study reports the successful synthesis of zinc-doped carbon dots (Zn-CDs) via a facile and environmentally benign hydrothermal route using citric acid, urea, and zinc nitrate as precursor materials. Comprehensive structural and optical characterization confirms the formation of uniformly dispersed, nearly spherical nanoparticles with an average size of 3.6 ± 0.5 nm and excellent colloidal stability in aqueous media. UV–visible absorption analysis reveals a red shift in the absorption maximum from 340 to 360 nm upon zinc incorporation, indicating modulation of π–π* electronic transitions. Correspondingly, the optical band gap decreases to 3.18 eV, suggesting enhanced charge carrier mobility and the generation of zinc-induced electronic defect states. Photoluminescence studies demonstrate a pronounced enhancement in optical performance, with emission intensity increasing by 52.8% and quantum yield improving by nearly threefold compared to undoped carbon dots. Successful zinc incorporation is further verified by FTIR and XPS analyses, which show the emergence of Zn–O vibrational bands around 420 cm^{-1} and characteristic Zn $2p_3/_2$ and Zn $2p_1/_2$ peaks at binding energies of 1022.1 eV and 1045.2 eV, respectively. Notably, Zn-CDs exhibit superior photostability, retaining approximately 95% of their initial fluorescence intensity under prolonged UV irradiation, whereas undoped carbon dots maintain only about 78%. This enhanced stability is attributed to Zn–O coordination, which effectively suppresses photo-oxidation and fluorescence quenching processes. The overall improvement in fluorescence behavior arises from a synergistic combination of band-gap narrowing (ΔEg = 0.24 eV), increased radiative recombination efficiency, and effective surface passivation of carboxyl and hydroxyl groups by Zn^{2+} ions. These effects collectively facilitate efficient radiative transitions and prolonged excited-state lifetimes, as evidenced by the increased average fluorescence lifetime of Zn-CDs (6.2 ns) compared to pristine carbon dots (4.1 ns). Owing to their strong emission, excellent aqueous solubility, biocompatibility, and enhanced photostability, the synthesized Zn-CDs show significant potential for applications in bioimaging, chemical sensing, and light-emitting devices. Moreover, the green, scalable, and heavy-metal-free synthesis strategy presented here offers a promising pathway for the development of sustainable photonic nanomaterials for industrial applications.

Competing Interests

There are no conflicts of interest exist among authors of this research paper.

ACKNOWLEDGEMENTS

Author Contributions

S.A; M.A.A & J.M. wrote the main manuscript Draft, writing, studied Data validation and Editing, Reviewing. All authors reviewed the manuscript outline.

Funding

No external fundings.

Data Availability

No data sets were generated or analysed during the current study.

REFERENCES

[1] Abbas, M. A. (2025). Advanced Synthesis and Multifunctional Characterization of Neodymium-Doped $Ba_2NiCoFe_{28-x}O_{46}$ X-Type Hexagonal Ferrites: A Comprehensive Study of Structural, Morphological, and Electromagnetic Properties. *Sch Acad J Biosci*, *8*, 1213-1227

[2] Abbas, M. A., Mahar, J., Hameed, N., & Rasool, M. S. (2025). DFT-Guided Design of a Low-Band-Gap Pyrazoline Scaffold: The Critical Role of a Para-Nitro Substituent. *Multidisciplinary Surgical Research Annals*, *3*(3), 461-503.

[3] Abbas, M. A., Mahar, J., Khan, M. J., Rasool, M. S., & Khan, M. Z. (2025). IN SILICO INVESTIGATION OF 3, 6-DIPHENYL-[1, 2, 4] TRIAZOLO [3, 4-B][1, 3, 4] THIADIAZOLE DERIVATIVES AS EGFR MODULATORS FOR LUNG CANCER TREATMENT. *The Cancer Research Review*, *4*(2), 243-308.

[4] Abbas, M. A., Mahar, J., Rasool, M. S., Khan, M. J., & Khan, M. Z. (2025). The Dual Therapeutic Promise of Quinoa: Exploring Antidiabetic and Antioxidant Effects through Experimental and Computational Models. *Multidisciplinary Surgical Research Annals*, *3*(3), 504-544.

[5] Ameen, S. S. M., Algethami, F. K., & Omer, K. M. (2025). Doping-enhanced luminescence of biowaste-derived carbon quantum dots for dual-mode Page 192 ratiometric and colorimetric detection of tetracycline. Journal of Inorganic and Organometallic Polymers and Materials, 1-13.

[6] Aslam, R., Wang, Q., Aslam, J., Mobin, M., Hussain, C. M., & Yan, Z. (2025). Effect of temperature and immersion time on the inhibition performance of Q235 steel using spent coffee grounds-derived carbon quantum dots: electrochemical, spectroscopic, and surface studies. Biomass and Bioenergy, 200, 107961.

[7] Chandrasekar, L. B., Sumathi, V., Ramya, D., Husain, A. J., Yuvaraj, S. A., Shankar, N., & Thirumalai, J. (2025). Influence of carbon quantum dots on enhanced capacitive behaviour of Cu-doped zinc oxide nanoparticles as electrodes in ultracapacitors. Applied Physics A, 131(12), 1034.

[8] Elzaablawy, R. S., Abdelazim, S., Ebeid, E. M., Eldaly, D. S. A., & El-Sawy, A. (2025). Synthesis and photocatalytic activity of zinc oxide/carbon quantum dots and zinc oxide/S-doped carbon quantum dots nanocomposites. Delta Journal of Science, 51(1), 114-129.

[9] ENYOH, C., Maduka, T., Qingyue, W., Suzuki, M., & Enyoh, I. (2025). Computational Biocompatibility and Safety Evaluation of Metal-Doped PET Carbon Quantum Dots via Multi-Target Molecular Docking and ADMET Analysis on Human Proteins.

[10] Gao, F., Fu, Q., Ruan, Y., Li, C., Wang, Y., Li, H., & Jiang, Y. (2025). Elucidating Manganese Single-Atom Doping: Strategies for Fluorescence Enhancement in Page 193 Water-Soluble Red-Emitting Carbon Dots and Applications for FL/MR Dual Mode Imaging. Advanced Science, 12(8), 2414895.

[11] Han, D., Liu, L., Liu, Z., Li, D., Chen, Y., Duan, Q., & Sang, S. (2023). Polyethyleneimine/polyethylene-glycol/Ti_3C_2Tx composites for ultrasensitive room-temperature CO_2 sensing. Sensors and Actuators B: Chemical, 393, 134221.

[12] Hosseinpanahi, K., Abbaspour-Fard, M. H., Goharshadi, E. K., Golzarian, M. R., Sajadi, S., & Vomiero, A. (2025). Enhanced optical properties of luminescent solar concentrators via metal ion doping in carbon dots. Journal of Materials Chemistry A, 13(17), 12639-12649.

[13] Jiang, W., Jiang, C., Liang, X., Mei, S., Zhang, Y., Feng, Y., & Liu, Y. (2025). Smart paper-based sensor: A novel bio-enzyme-free dual-mode platform for real-time visual monitoring of organophosphorus pesticides. Chemical Engineering Journal, 169503.

[14] Kapoor[1], D. N., & Sheth, S. (2024). Progress in drug delivery and diagnostic applications of carbon. Nanoscience Editor's Pick 2024.

[15] Li, Z., Jiao, T., Li, W., Wang, Z., Chang, Y., Shen, R., & Du, G. (2024). Surface chemical composition and HRTEM analysis of heteroepitaxial β-Ga_2O_3 films grown by MOCVD. Applied Surface Science, 652, 159327.

[16] Moeini, A., Ghiasi, A., Abadi, M. D. M., Khachatourian, A. M., Hosseini, H. R. M., & Malek, M. (2025). Zn-doped superparamagnetic iron oxide nanoparticles LCysteine functionalised N-doped graphene quantum dots as multifunctional contrast agents for dual-model imaging (MRI & FI). Materials & Design, 114269.

[17] Ou, S., Qing, M., Mu, Z., Yuan, Y., Li, Y., & Bai, L. (2025). Enhanced electrochemiluminescence aptasensor using ZnO as the co-reaction accelerator of the Mn-NHCDs/TEA system for the detection of florfenicol. Microchimica Acta, 192(10), 1-13.

[18] Patra, D., Saini, A., Bag, M., & Singh, S. P. (2024). Amine-free $CsPbBr_3$ perovskite nanocrystals with a near-unity photoluminescence quantum yield for a superfast photodetector. ACS Applied Nano Materials, 7(14), 16438-16449.

[19] Priyadharshini, A., & Napoleon, A. A. (2025). Dual co-doped fluorescent carbon dots for ultra-sensitive detection of Co2+ ions: Applications in food samples, bioimaging, and environmental monitoring. Inorganic Chemistry Communications, 114716.

[20] Ran, N. N., Luo, Q., Li, H. W., & Wu, Y. (2025). A novel fluorescence nanoprobe for unique determination of chlorotetracycline based on zinc-doped carbon dots. Colloids and Surfaces A: Physicochemical and Engineering Aspects, 137935.

[21] Simiyon, G. G., Nivetha, B., Vergheese, T. M., & Jayaprakash, N. (2025). Novel photodamage-free bioimaging and anticancer studies using ultra-bright near infrared-emitting nitrogen-doped carbon dots intercalated with Zn $(OH)_2$ nanosheets. Chemical Papers, 79(4), 2629-2636.

[22] Swami, S., Joshi, A., Singh, G., Rai, A. K., Singh, S. K., & Singh, D. K. (2025). Facile synthesis and characterisation of transition metal-doped carbon dots (TMDCDs) for efficient photocatalytic degradation of methylene blue. Journal of Molecular Structure, 143467.

[23] Xie, J., Cao, Q., Li, L., Wang, W., Pan, Y., Wei, X., & Li, Y. (2023). A double perovskite Mn^{4+}-doped Sr_2ScNbO_6 phosphor for indoor plant growth lighting. Optical Materials, 143, 114212.

[24] Zhang, Y., Guo, Y., Sun, K., Li, X., Liu, X., Zhu, J., & Khan, M. Z. H. (2025). Mechanism of Fluorescence Characteristics and Application of Zinc-Doped Carbon Dots Synthesized by Using Zinc Citrate Complexes as Precursors. C, 11(3), 48.

[25] Abbas, M. A. (2025). Advanced Synthesis and Multifunctional Characterization of Neodymium-Doped $Ba_2NiCoFe_{28-x}O_{46}$ X-Type Hexagonal Ferrites: A Comprehensive Study of Structural, Morphological, and Electromagnetic Properties. *Sch Acad J Biosci*, *8*, 1213-1227

[26] Abbas, M. A., Mahar, J., Hameed, N., & Rasool, M. S. (2025). DFT-Guided Design of a Low-Band-Gap Pyrazoline Scaffold: The Critical Role of a Para-Nitro Substituent. *Multidisciplinary Surgical Research Annals*, *3*(3), 461-503.

[27] Abbas, M. A., Mahar, J., Khan, M. J., Rasool, M. S., & Khan, M. Z. (2025). IN SILICO INVESTIGATION OF 3, 6-DIPHENYL-[1, 2, 4] TRIAZOLO [3, 4-B][1, 3, 4] THIADIAZOLE DERIVATIVES AS EGFR MODULATORS FOR LUNG CANCER TREATMENT. *The Cancer Research Review*, *4*(2), 243-308.

[28] Abbas, M. A., Mahar, J., Rasool, M. S., Khan, M. J., & Khan, M. Z. (2025). The Dual Therapeutic Promise of Quinoa: Exploring Antidiabetic and Antioxidant Effects through Experimental and Computational Models. *Multidisciplinary Surgical Research Annals*, *3*(3), 504-544.

[29] Abbas, M. A., Junaid, M. J. M., Rasool, M. S., & Mahar, J. (2025). Structural and NLO Properties of Novel Organic 4-Bromo-4-Nitrostilbene Crystal: Experimental and DFT Study. *International Research Journal of Management and Social Sciences*, *6*(4), 1-20.

[30] Abbas, M. A., Khan, M. Z., Atif, H. M., Shahzad, A., & Mahar, J. (2025). Computer-Aided Analysis of Oxino-bis-Pyrazolederivative as a Potential Breast Cancer Drug Based on DFT, Molecular Docking, and Pharmacokinetic Studies: Compared with the Standard Drug Tamoxifen. *Indus Journal of Bioscience Research*, *3*(6), 535-537.

[31] Ghafoor, A., Abbas, M. A., Ahmad, J., Ali, R., Abbas, M., Ahmad, A., ... & Masood, H. T. (2025). Synthesis and characterization of pyranopyrazole derivatives as potential organic nonlinear optical (NLO) materials and density functional theory (DFT) studies. *FRONTIERS IN CHEMICAL SCIENCES*, *6*(2), 103-116.

[32] Rasool, M. S., Abbas, M. A., Khan, M. J., Mahar, J., & Khan, M. Z. IDENTIFICATION OF NATURAL EGFR TYROSINE KINASE INHIBITORS FROM CHENOPODIUM QUINOA WILLD. VIA COMBINATORIAL IN SILICO AND PHARMACOLOGICAL SCREENING.

[33] Ghafoor, A., Amir, M., Abass, J. A., Abbas, M., Shabbir, S., Ali, R., & Ahmad, N. Molecular Structure, Electronic and Topology of Pyranopyrazole Derivatives and their Molecular Docking with DNA and Protein to evaluate Anticancer Potential.